




Comparison of strange particle production measurements in central Pb–Pb collisions at $\sqrt{s_{NN}} = 2.76$ and 5.02 TeV by using Monte Carlo simulation models EPOS-1.99 and EPOS-LHC

Atif Arif^{1,2,a} , Y. Ali¹, Mahnaz Q. Haseeb¹

¹ Department of Physics, COMSATS University Islamabad, Park Road, Islamabad 44000, Pakistan

² Department of Physics, Govt. Gordon College, Rawalpindi, Pakistan

Received: 21 September 2021 / Accepted: 19 April 2022

© The Author(s), under exclusive licence to Società Italiana di Fisica and Springer-Verlag GmbH Germany, part of Springer Nature 2022

Abstract The present paper is a comparative study of transverse momentum spectra of K_s^0 – mesons, Λ – hyperons, multi-strange baryons Ξ^- , Ξ^+ , Ω^- and Ω^+ in the most central Pb–Pb collisions at $\sqrt{s_{NN}} = 2.76$ and 5.02 TeV for the mid rapidity interval $|y| < 0.5$ by using two different Monte Carlo simulation models, EPOS-1.99 and EPOS-LHC. Particle ratios Λ/K_s^0 are studied at the two center-of-mass energies to understand the enhancement of heavier hadrons over the lighter ones. Nuclear modification factors are also constructed for multi-strange baryons at $\sqrt{s_{NN}} = 2.76$ TeV to study particle production and energy loss mechanisms. The validity of these models is tested for Pb–Pb collisions at $\sqrt{s_{NN}} = 2.76$ and 5.02 TeV by comparing the simulation data with ALICE experimental data.

1 Introduction

The measurement of strange and multi-strange particles provides us insights into the extremely hot and dense state of matter called Quark Gluon Plasma (QGP), which is studied by heavy ion collision experiments such as at the Relativistic Heavy Ion Collider (RHIC) and the Large Hadron Collider (LHC) [1–3]. The final state particles are the product of the evolution of the system through different stages which shows a transition from the hadronic phase to the deconfined state of QGP and then back to a confined hadron state. The properties of this hot and dense medium can be characterized by studying the energy loss of quarks and gluons traversing the QCD medium [4]. At high transverse momenta, hadron production is suppressed because of parton energy loss. The study of high p_T spectra is helpful to understand the perturbative QCD (pQCD).

A systematic study of strangeness production is one of the fundamental interests for investigating the thermal properties of QCD matter produced in heavy ion collision experiments [5]. The enhanced production of strange quarks is predicted as a signature of the formation of QGP [6]. The possible reasons of strangeness enhancement in the central A – A collisions are due to large baryon densities and large temperatures expected to be achieved. The hadron resonance gas model (HRGM) predicts different chemical freeze-outs for strange and non-strange hadrons [7]. The production of s quarks is predicted to be suppressed in pp , p – A and peripheral A – A [6]. The study of strange particle production also helps to understand the non-perturbative QCD aspects, e.g., parton interactions and hadronization.

Heavy ion collision processes can be divided into hard and soft ones. The soft or low transverse momentum processes, also known as thermal-like processes, are responsible for multi-parton interactions, while the hard or high transverse momentum processes are produced by either single or a few parton exchanges. Soft processes are described by the “exponential law equation,” while hard processes are described by “power law equation” [8–11]. It is observed in high-energy collision experiments that the yields of high p_T particles produced in Pb–Pb collisions are generally suppressed as compared to pp collisions. Bjorken suggested that the observed suppression of charged particle production at high p_T in Pb–Pb collisions is an effect due to the partons energy loss, while they propagate through strongly interacting medium [12, 13].

The modification of high p_T particle production in A – A collisions is quantified by studying an important observable called nuclear modification factor (NMF) R_{AA} that is defined as:

$$R_{AA} = \frac{dN^{AA}/dp_T}{\langle N_{\text{Coll}} \rangle dN^{pp}/dp_T}$$

Nuclear modification factor (NMF) R_{AA} is a ratio of particle differential yield in A – A collisions to that of pp collisions scaled by the average number of binary nucleon–nucleon collisions $\langle N_{\text{Coll}} \rangle$. The study of R_{AA} gives some very important information about

^a e-mail: atif_arif_physics@yahoo.com (corresponding author)

the properties of the background medium formed as a result of pp and A – A interactions. If A – A collisions are a simple superposition of elementary nucleon–nucleon collisions, then R_{AA} is equal to unity which shows the absence of nuclear effects. However for $R_{AA} < 1$, there could be a possible suppression of particle production compared to binary–collisions scaling which takes place due to an effect known as jet quenching of partons [12].

The measurements of R_{AA} for charged particles as a function of p_T at the LHC [14–17] have shown that in central Pb–Pb collisions at $\sqrt{s_{NN}} = 2.76$ TeV the particle yields are suppressed by a factor of up to 7 for p_T range of 6–7 GeV/c, but the suppression decreases for larger p_T . In 2015 LHC had its first Pb–Pb collisions at $\sqrt{s_{NN}} = 5.02$ TeV and observed nearly the same amount of suppression for central Pb–Pb collisions within the same p_T range [18]. The results of CMS Collaboration on charged particles for R_{AA} at $\sqrt{s_{NN}} = 5.02$ TeV have shown a similar amount of suppression in charged particle production for $p_T = 6$ –9 GeV/c in the central Pb–Pb collisions [19].

As the strange quark is heavier than up and down quarks, the production of strange hadrons is generally suppressed relative to hadrons containing lighter quarks. The amount of strangeness suppression is important to understand which of the Monte Carlo simulation models, which are based on different theoretical calculations, is more likely to explain the observed suppression. The comparison of yields of high p_T particles produced in Pb–Pb collisions with the predictions of theoretical models gives very important insights about the fundamental properties of QGP. As the threshold for strange quark production in quark-gluon plasma is much smaller than in a hadron gas, an enhancement in strangeness production is considered to be an indication of QGP [20].

The identified particle spectra at low p_T and high center of mass energy are helpful to understand the predictions of hydrodynamic models. The experimental data show significant variation from models at intermediate p_T range; 2–10 GeV/c. Within this p_T range, several hadronization models have been proposed especially to explain enhancement of heavy hadrons over the lighter ones [21–23]. Few models suggest that enhancement of heavier hadrons over lighter hadrons at intermediate p_T is expected from the collective hydrodynamic expansion of the system [24–26]. This ratio is further enhanced at intermediate p_T in parton coalescence models [27–29], which inter account radial flow as well, suggesting that coalescence of lower p_T quarks could be responsible for the production of baryons with larger p_T than for mesons, although the decrease in the baryon-to-meson ratio at high p_T is due to an effect called parton fragmentation.

The present work is in continuation of our previous work in which we studied the transverse momentum distributions of some selected charged particles at LHC and RHIC energies [30–32]. The current paper is based on the comparative study of transverse momentum spectra of some selected strange particles such as K_s^0 – mesons, Λ – hyperons and multi-strange baryons (Ξ^- , Ξ^+ , Ω^- and Ω^+) at two different LHC energies, i.e., $\sqrt{s_{NN}} = 2.76$ and 5.02 TeV for MC simulation models EPOS-1.99 and EPOS-LHC. For this purpose, 100 k Pb–Pb collision events are generated at two LHC energies $\sqrt{s_{NN}} = 2.76$ and 5.02 TeV for mid-rapidity interval ($|\eta| < 0.5$). Particle ratios Λ/K_s^0 are also studied at the two energies to understand the baryon-to-meson ratio. Nuclear modification factors are constructed for multi-strange baryons at $\sqrt{s_{NN}} = 2.76$ TeV to understand particle production and energy loss mechanisms. This gives an overall picture of the models predictions for strange particles at the two particular LHC energies for Pb–Pb collision. The distributions obtained from the simulation codes are also compared with ALICE experimental data for strangeness production in Pb–Pb collisions at $\sqrt{s_{NN}} = 2.76$ TeV and $\sqrt{s_{NN}} = 5.02$ TeV [18, 33, 34].

The paper is organized as follows. A description of simulation models is given in the next section. Transverse momentum distributions of strange and multi-strange baryons along with the particle ratios and nuclear modification factors as a function of transverse momentum are shown in the results and discussion section. The last section focuses on conclusions.

2 Method and models

We have used two different hadron production MC event generators: EPOS-1.99 and EPOS-LHC [35–37], for the study of p_T distributions of strange and multi-strange hadrons produced in central Pb–Pb collisions at $\sqrt{s_{NN}} = 2.76$ and 5.02 TeV, and we compared their predictions with the ALICE measurements.

EPOS stands for energy conserving quantum mechanical multiple scattering approach, based on partons (parton-ladder), off-shell remnants, and splitting of parton ladders [36]. It is purely constructed on theoretical basis, critically tested and verified over existing hadronic data. EPOS is a model based on parton model including binary parton-parton collisions, and each of these collisions produces a separate parton ladder [37]. For the cross section calculations and particle yields, energy conservation is employed in the EPOS model. However, energy conservation is not considered for cross section calculations in other models [38]. EPOS is a quantum mechanical model which inter-accounts multiple scattering based on partons and strings. Besides being used for cosmic rays, it is also used to simulate data for heavy ion physics experiments such as the ones at SPS, LHC and RHIC. EPOS-1.99 deals mostly with the soft interactions with its emphasis on the high partons densities which are significant for nucleus-nucleus (A – A) collisions. An upgraded version of EPOS-1.99 is also developed to inter-account LHC energies; it is known as EPOS-LHC [39]. This new version of EPOS model can reproduce all minimum bias results for all the particles with transverse momentum up to a few GeV/c. By using these models, we have generated and then analyzed our simulated data.

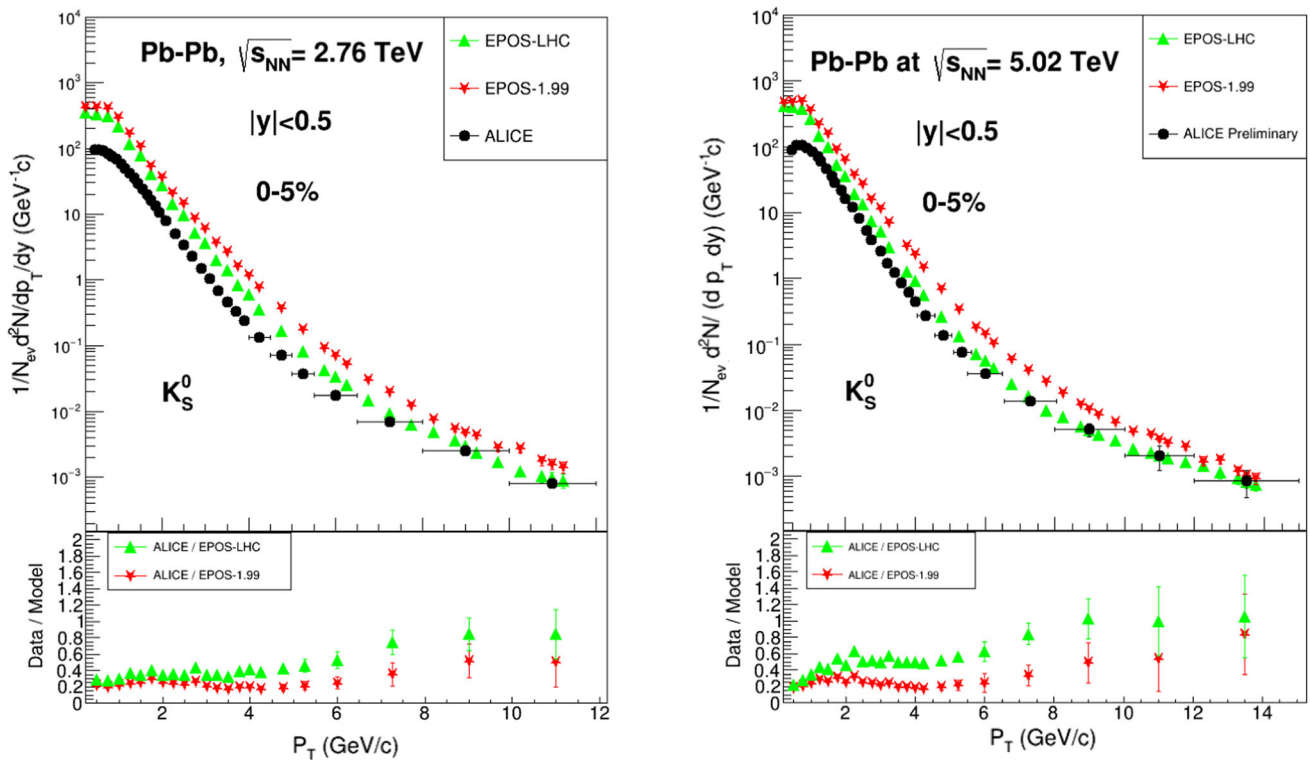


Fig. 1 Transverse momentum distribution of K_s^0 – mesons produced in the most central Pb–Pb collision at $\sqrt{s_{NN}} = 2.76$ TeV (left panel) and 5.02 TeV (right panel) for MC simulation models and ALICE data. The vertical lines show statistical errors, and the horizontal lines represent the bin width. Lower panel shows ALICE data to MC model ratios

3 Results and discussion

We study the transverse momentum distribution of strange and multi-strange particles produced in most central Pb–Pb collision at $\sqrt{s_{NN}} = 2.76$ and 5.02 TeV in the mid rapidity interval ($-0.5 < y < 0.5$) for Monte Carlo simulation models EPOS-1.99 and EPOS-LHC. Transverse momentum distributions of K_s^0 – mesons and Λ – hyperons produced in the most central Pb–Pb collisions at $\sqrt{s_{NN}} = 2.76$ TeV and 5.02 TeV for the simulation codes EPOS-LHC and EPOS-1.99 along with ALICE experimental data are plotted in Figs. 1 and 2, respectively. Comparison of transverse momentum distributions at the two center-of-mass energies 2.76 TeV and 5.02 TeV for Ω^- and $\bar{\Omega}^+$ is presented in Figs. 3 and 4, respectively. Similarly, transverse momentum distributions of multi-strange hadrons Ξ^- and $\bar{\Xi}^+$ for central Pb–Pb collision at $\sqrt{s_{NN}} = 2.76$ TeV and 5.02 TeV are presented in Figs. 5 and 6, respectively. Figure 7 displays the nuclear modification factors of multi-strange particles ($\Xi^- + \bar{\Xi}^+$) and ($\Omega^- + \bar{\Omega}^+$) at $\sqrt{s_{NN}} = 2.76$ TeV. Figure 8 shows the baryon-to-meson ratios Λ/K_s^0 as a function of p_T at $\sqrt{s_{NN}} = 2.76$ and 5.02 TeV. Data to MC model ratios are shown in the lower panels in each case.

From Fig. 1 (left panel), one can see that the predictions of EPOS-LHC are much higher than the ALICE data for K_s^0 – mesons at low transverse momentum, i.e., $p_T < 7$ GeV/c. However, with the increase in the center-of-mass energy from $\sqrt{s_{NN}} = 2.76$ TeV to 5.02 TeV, the predictability of the model improves. EPOS-LHC satisfactorily explains the experimental data at high p_T , i.e., for $p_T > 7$ GeV/c. On the other hand, EPOS-1.99 clearly overestimates the yields of K_s^0 in the whole p_T range. However, at high p_T , i.e., $p_T > 9$ GeV/c, its predictions converge toward the experimental data. It is important to note that both the models overestimate in the well-known interval of jet suppression. Therefore, both of these models could not explain the region of jet suppression for K_s^0 – mesons.

Figure 2 shows the transverse momentum distribution of Λ – hyperons produced in the most central Pb–Pb collisions at $\sqrt{s_{NN}} = 2.76$ TeV (left panel) and 5.02 TeV (right panel) for MC simulation models EPOS-1.99 and EPOS-LHC. It can be seen that EPOS-LHC predictions are not satisfactory at low transverse momenta, i.e., $p_T < 2$ GeV/c, where thermal processes dominate. Although it satisfactorily explains the ALICE experimental data for $p_T > 2$ GeV/c at $\sqrt{s_{NN}} = 2.76$ TeV and 5.02 TeV, EPOS-1.99 predictions are not satisfactory for $p_T < 7$ GeV/c and overestimate the yield of Λ – hyperons in this p_T range. However, with the increase in the transverse momentum, its predictions start improving and come close to the ALICE data for $p_T > 7$ GeV/c. This shows that at high p_T EPOS-1.99 describes data better as compared to its behavior at low p_T .

Figure 3 presents the p_T -distribution of Ω^- produced in central Pb–Pb collisions at $\sqrt{s_{NN}} = 2.76$ TeV (left panel) and 5.02 TeV (right panel). One can see that EPOS-LHC is able to explain the ALICE data at low $p_T < 3$ GeV/c for both the selected center-of-mass

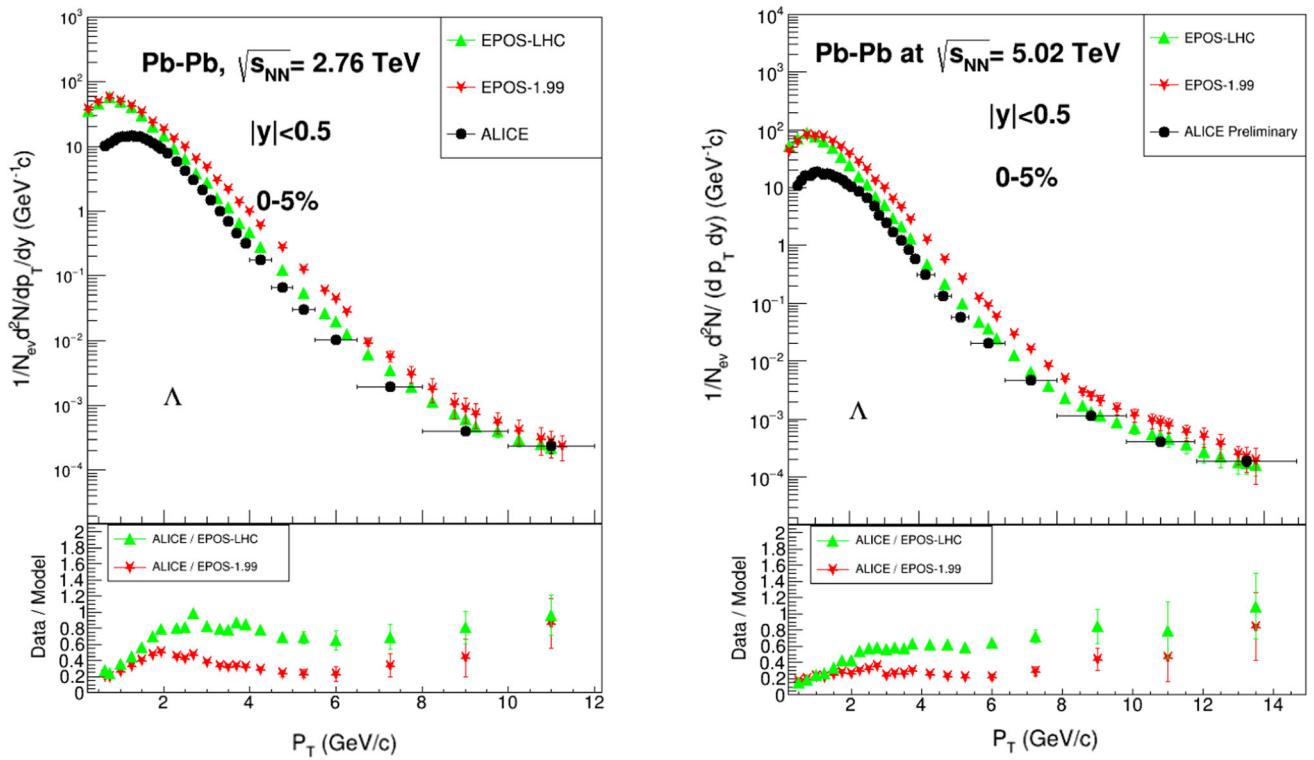


Fig. 2 Transverse momentum distribution of Λ – hyperons produced in the most central Pb–Pb collision at $\sqrt{s_{NN}} = 2.76$ TeV (left panel) and 5.02 TeV (right panel) for MC simulation models and ALICE data. The vertical lines show statistical errors, and the horizontal lines represent the bin width. Lower panel shows ALICE data to MC model ratios

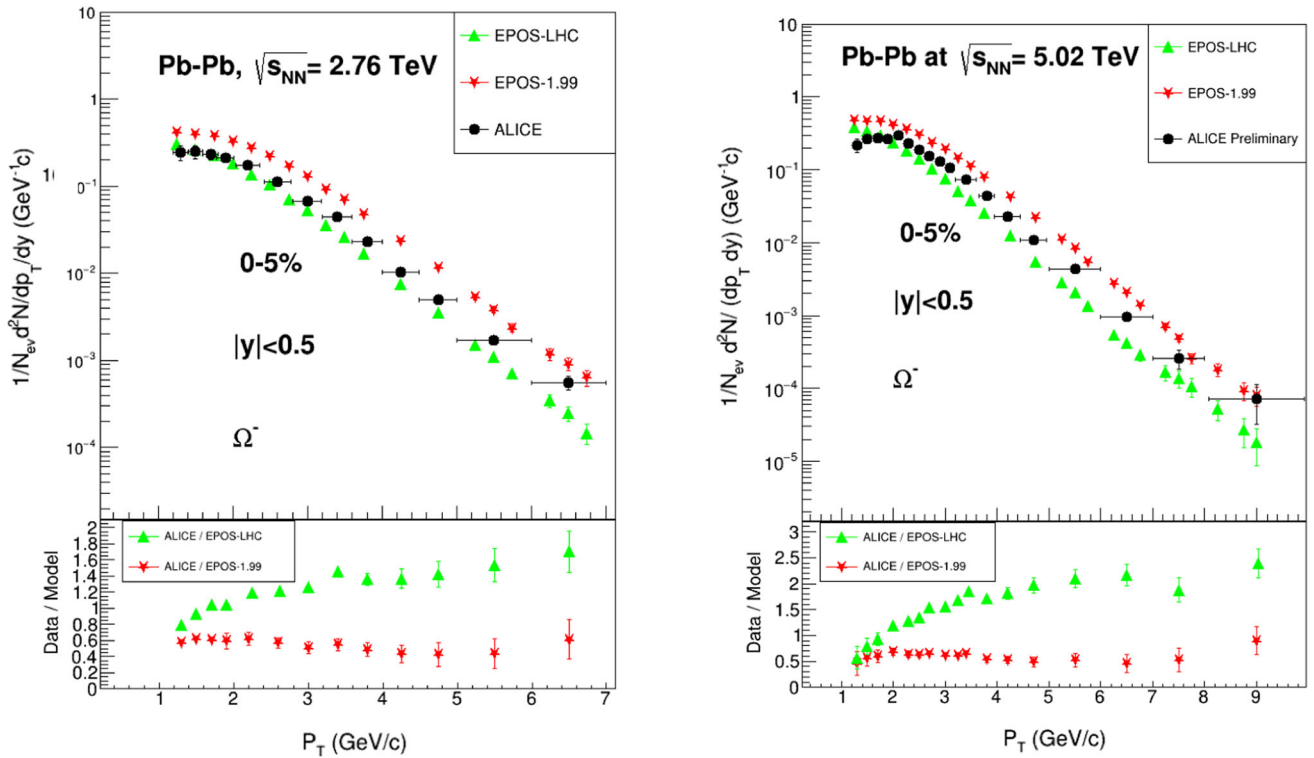


Fig. 3 Transverse momentum distribution of Ω^- produced in the most central Pb–Pb collision at $\sqrt{s_{NN}} = 2.76$ TeV (left panel) and 5.02 TeV (right panel) for MC simulation models EPOS1.99, EPOS-LHC and ALICE data. The vertical lines show statistical errors, and the horizontal lines represent the bin width. Lower panel shows ALICE data to MC model ratios

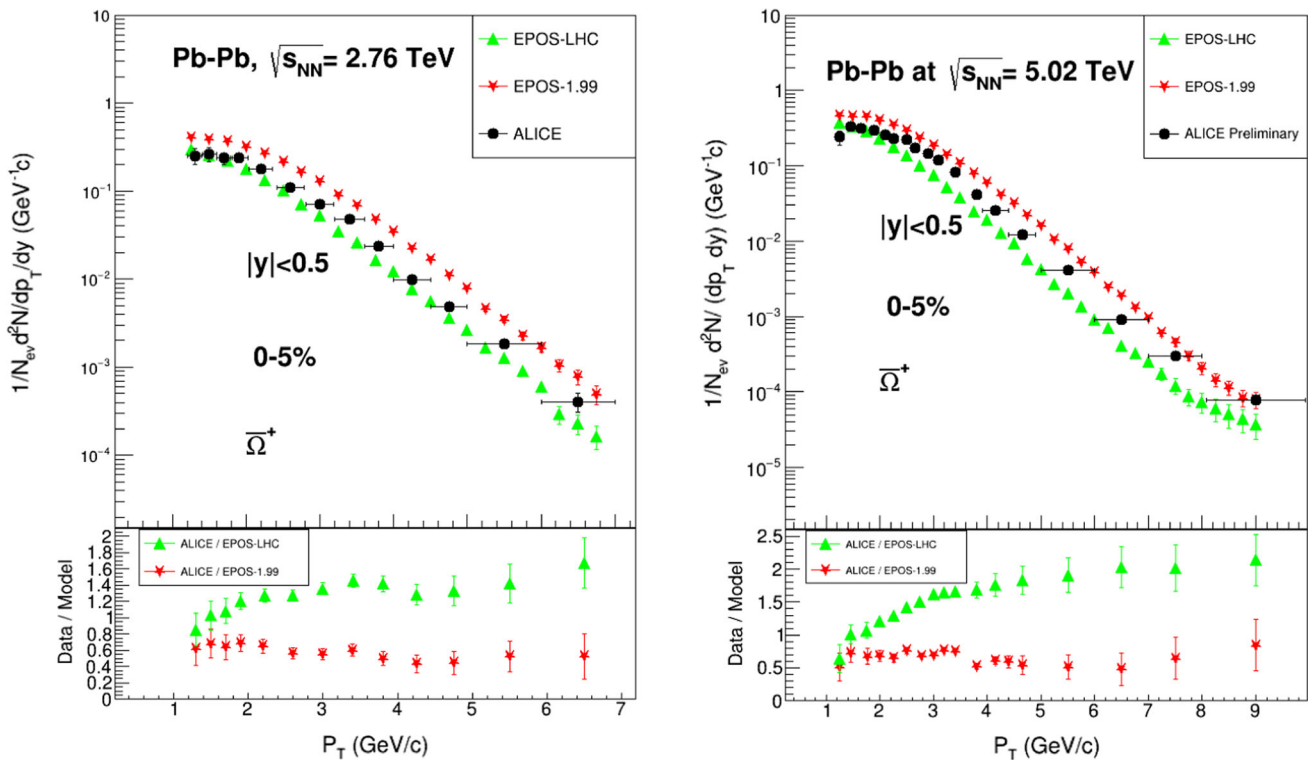


Fig. 4 Transverse momentum distribution of $\bar{\Omega}^+$ produced in the most central Pb–Pb collision at $\sqrt{s_{NN}} = 2.76$ TeV (left panel) and 5.02 TeV (right panel) for MC simulation models and ALICE data. The vertical lines show statistical errors, and the horizontal lines represent the bin width. Lower panel shows ALICE data to MC model ratios

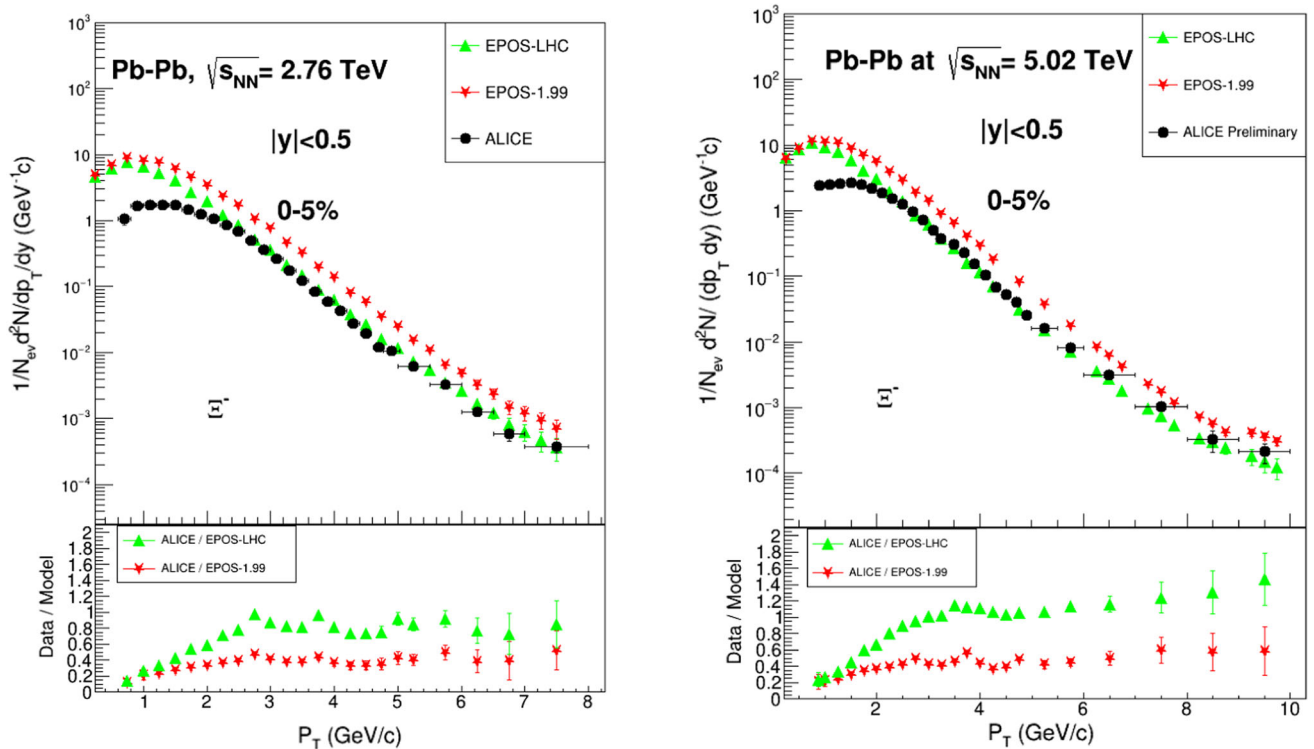


Fig. 5 Transverse momentum distribution of Ξ^- produced in the most central Pb–Pb collision at $\sqrt{s_{NN}} = 2.76$ TeV (left panel) and 5.02 TeV (right panel) for MC simulation models and ALICE data. The vertical lines show statistical errors, and the horizontal lines represent the bin width. Lower panel shows ALICE data to MC model ratios

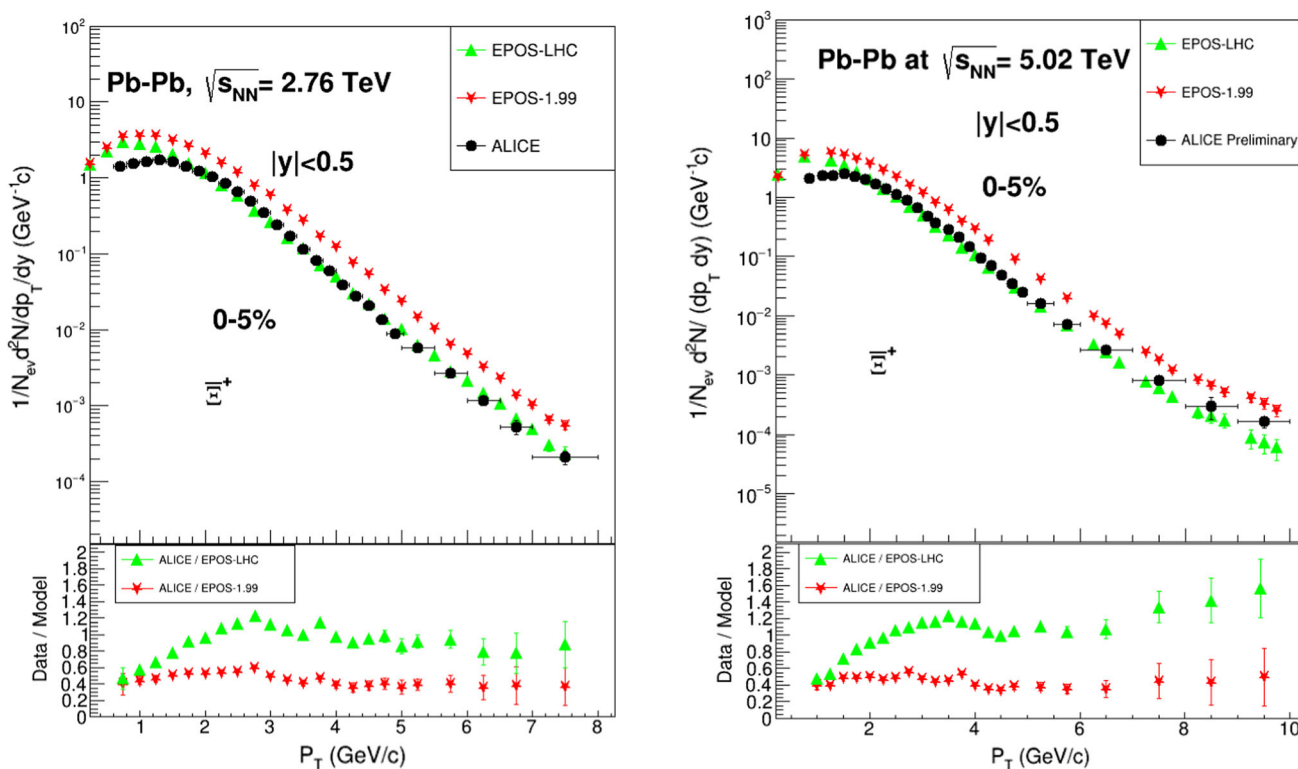


Fig. 6 Transverse momentum distribution of Ξ^+ produced in the most central Pb–Pb collision at $\sqrt{s_{NN}} = 2.76$ TeV (left panel) and 5.02 TeV (right panel) for MC simulation models and ALICE data. The vertical lines show statistical errors, and the horizontal lines represent the bin width. Lower panel shows ALICE data to MC model ratios

energies. However, it starts deviating from ALICE data for $p_T > 3$ GeV/c. On the other hand, EPOS-1.99 overestimates the ALICE data for the entire p_T range at $\sqrt{s_{NN}} = 2.76$ TeV. However, for the center-of-mass energy 5.02 TeV, EPOS-1.99 predictions are relatively closer to the ALICE data at high $p_T > 7$ GeV/c.

Figure 4 shows the p_T -distribution of Ξ^+ produced in central Pb–Pb collision at $\sqrt{s_{NN}} = 2.76$ TeV (left panel) and 5.02 TeV (right panel). It can be seen that with the increase in center-of-mass energy from 2.76 to 5.02 TeV, we notice that EPOS-1.99 predictions start improving. At high $p_T > 7$ GeV/c EPOS-1.99 predictions converge toward ALICE experimental data. On the other hand, with the increase in energy, EPOS-LHC start deviating from the ALICE data. However, its predictions are still valid for $p_T < 3$ GeV/c.

Figure 5 shows the transverse momentum distribution of Ξ^- produced in the most central Pb–Pb collisions at $\sqrt{s_{NN}} = 2.76$ TeV (left panel) and 5.02 TeV (right panel). One can see that the predictions of EPOS-LHC are higher than the ALICE data for the yield of Ξ^- at low transverse momentum in the interval of $p_T < 2$ GeV/c at both the center-of-mass energies. However, it satisfactorily explain the ALICE data in the interval $2 < p_T < 7.5$ GeV/c. On the other hand, EPOS-1.99 overestimates the yield of Ξ^- for the entire p_T range for both the center-of-mass energies, though it gives only quantitative predictions and is able to explain quantitatively the behavior of the differential yields in the whole high p_T region.

Figure 6 shows the transverse momentum distribution of Ξ^+ produced in the most central Pb–Pb collisions at $\sqrt{s_{NN}} = 2.76$ TeV (left panel) and 5.02 TeV (right panel). It can be seen from Fig. 6 that the predictions of EPOS-LHC for the yield of Ξ^+ are higher than the ALICE data at low transverse momentum, i.e., for $p_T < 1.5$ GeV/c for both center-of-mass energies. However, it satisfactorily explains the ALICE data in the interval $2 < p_T < 7.5$ GeV/c at both center-of-mass energies and underestimates for $p_T > 7.5$ GeV/c at $\sqrt{s_{NN}} = 5.02$ TeV. On the other hand, EPOS-1.99 overestimates the yield of Ξ^+ for the entire p_T range. It explains quantitatively the behavior of the yield in the entire high p_T region ($2 < p_T < 7.5$ GeV/c).

Figure 7 shows the distribution of the nuclear modification factor for multi-strange particles $\Xi^- + \Xi^+$ (right panel) and $\Omega^- + \Omega^+$ (left panel) as a function of transverse momentum for the most central Pb–Pb collisions at $\sqrt{s_{NN}} = 2.76$ TeV using MC simulation models EPOS-LHC and EPOS-1.99. It is clear from Fig. 7 that EPOS-LHC nicely explains the entire distribution of R_{AA} for $\Omega^- + \Omega^+$ and $\Xi^- + \Xi^+$. EPOS-1.99 in contrast is able to explain the distribution of R_{AA} for $\Omega^- + \Omega^+$ and $\Xi^- + \Xi^+$ only at low transverse momenta, i.e., $p_T < 4$ GeV/c and $p_T < 3$ GeV/c, respectively. Its predictions are higher than the ALICE data in the region of jet suppression where the nuclear modification factor shows a decreasing trend, i.e., in the interval: $4 < p_T < 7$ GeV/c.

Figure 8 shows the comparison of strange particle ratio Λ/K_s^0 as a function of transverse momentum for the most central Pb–Pb collisions at $\sqrt{s_{NN}} = 2.76$ and 5.02 TeV for simulation models EPOS-LHC and EPOS-1.99. Their distributions show that the

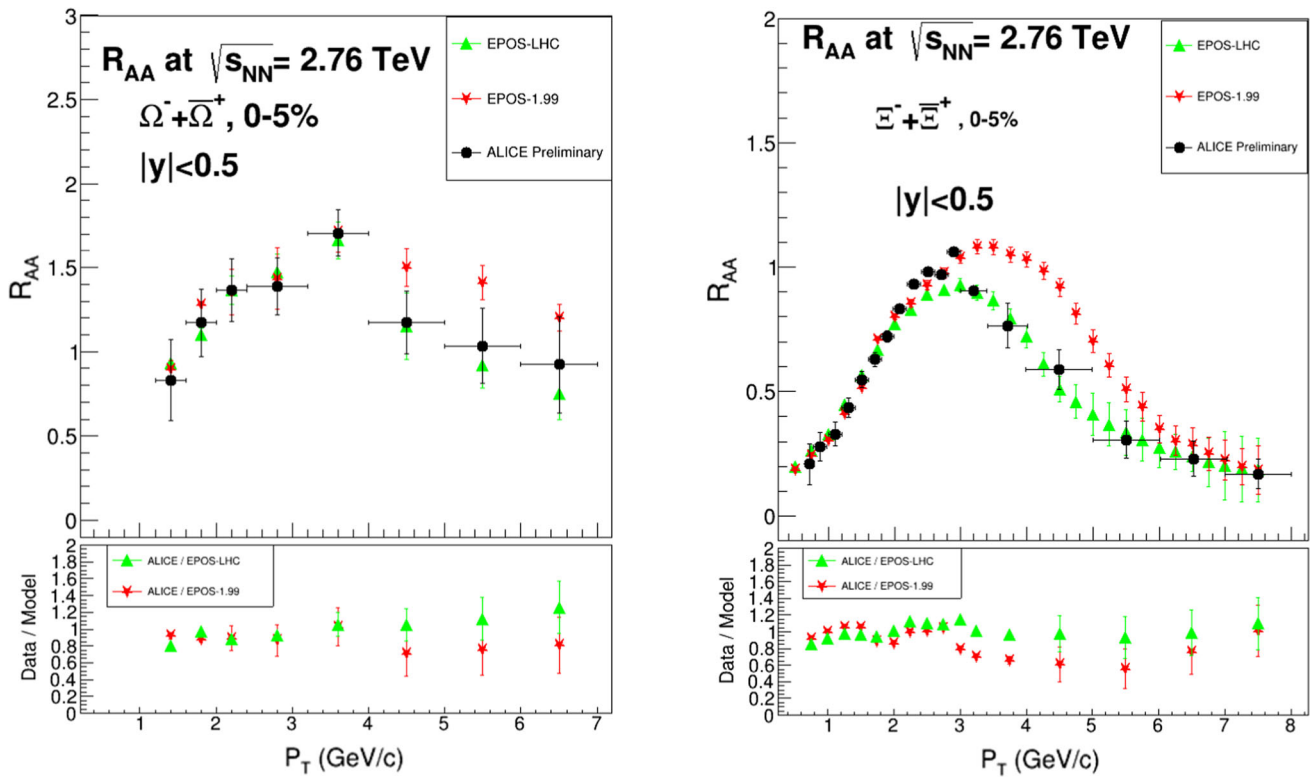


Fig. 7 Nuclear modification factor of multi-strange particles $\Xi^- + \Xi^+$ and $\Omega^- + \Omega^+$ produced in the most central Pb–Pb collisions at $\sqrt{s_{NN}} = 2.76$ TeV as a function of p_T for MC simulation models and ALICE data. The vertical lines show statistical errors, and the horizontal lines represent the bin width. Lower panel shows ALICE data to MC model ratios

predictions of the two models are similar. Both the models explain the experimental data at low $p_T < 4$ GeV/c, where the ratio Λ/K_s^0 shows a rising trend. However, both the simulation models overestimate the experimental data in the region of jet suppression: $4 < p_T < 7$ GeV/c.

4 Conclusion

The transverse momentum spectra of K_s^0 – mesons, Λ – hyperons and multi-strange particles: Ξ^- , Ξ^+ , Ω^- and Ω^+ have been studied in the most central Pb–Pb collisions at $\sqrt{s_{NN}} = 2.76$ and 5.02 TeV for the mid rapidity interval $|y| < 0.5$ by using two different Monte Carlo simulation models: EPOS-1.99 and EPOS-LHC. The validity of simulation codes of these models is tested by comparing the simulation data with the ALICE experimental data. We can conclude that:

- EPOS-LHC explains the yield of K_s^0 – mesons at high p_T , i.e., for $p_T > 7$ GeV/c. On the other hand, EPOS-1.99 clearly overestimates the yields of K_s^0 in the whole p_T range.
- For Λ – hyperons EPOS-LHC satisfactorily explains the ALICE data for $p_T > 2$ GeV/c at both center-of-mass energies. However, EPOS-1.99 only works well at high $p_T > 7$ GeV/c.
- For Ω^- and Ω^+ EPOS-LHC is able to explain the ALICE data at low $p_T < 3$ GeV/c; however, it shows some energy dependence. EPOS-1.99 overestimates the ALICE data for $p_T < 7$ GeV/c, although at high $p_T > 7$ GeV/c EPOS-1.99 predictions converge toward ALICE data.
- For Ξ^- and Ξ^+ the predictions of EPOS-LHC are higher than the ALICE data at low p_T in the interval of $p_T < 2$ GeV/c. EPOS-LHC can explain the behavior of the yields in the interval of recombination ($2 < p_T < 4$ GeV/c) and jet suppression ($4 < p_T < 7$ GeV/c) at both center-of-mass energies. On the other hand, EPOS-1.99 is unable to give satisfactory predictions for these particle yields in these intervals.
- The behavior of the ratio Λ/K_s^0 as a function of transverse momentum could not be properly reproduced by both models in the jet suppression region ($4 < p_T < 7$ GeV/c).
- EPOS-LHC can explain the behavior of R_{AA} for multi-strange particles $\Xi^- + \Xi^+$ and $\Omega^- + \Omega^+$, but EPOS-1.99 model gets in problem to describe the behavior of R_{AA} of these particles in the p_T interval 3–7 GeV/c.

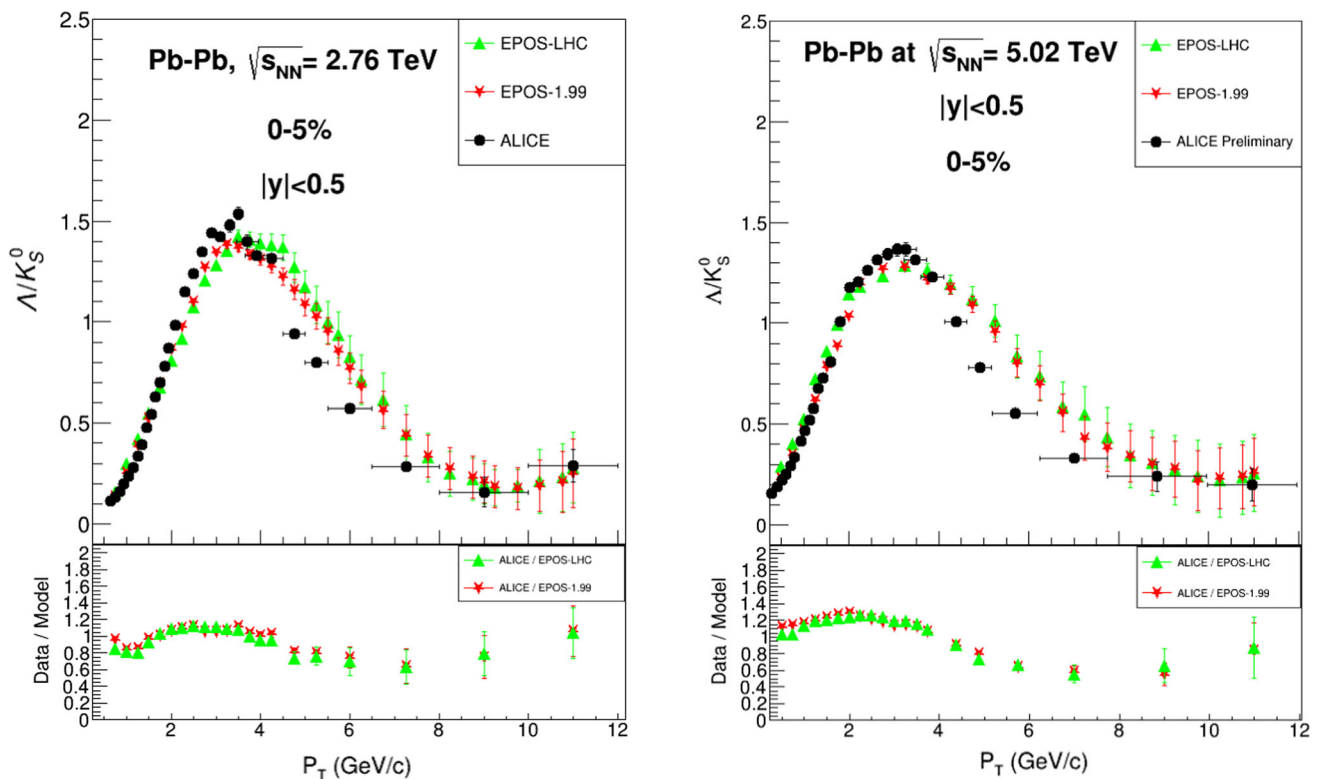


Fig. 8 Transverse momentum distribution of Λ/K_S^0 in the most central Pb–Pb collision at $\sqrt{s_{NN}} = 2.76$ TeV (left panel) and 5.02 TeV (right panel) for MC simulation models and ALICE data. The vertical lines show statistical errors, and the horizontal lines represent the bin width. Lower panel shows ALICE data to MC model ratios

Reference [33] gave a comparison with models at $\sqrt{s_{NN}} = 2.76$ TeV that suggests that the behavior at low transverse momenta $p_T \leq 2$ GeV/c is explained by hydrodynamical models, while the peak at intermediate range of the momenta $2 < p_T < 4$ GeV/c is qualitatively explained by recombination models, the intermediate p_T range $4 < p_T < 7$ GeV/c can be identified as the region of jet suppression, while the hard processes relevant at $p_T > 7$ GeV/c provide significant information on fragmentation [40]. EPOS-LHC model [41] describes the dependence over the entire transverse momentum range since it incorporates not only radial flow but also the interactions of jets with the medium.

Acknowledgements We acknowledge the COMSATS University Islamabad, Islamabad campus, Pakistan, which provided all possible facilities and a suitable platform to perform the simulations and analysis.

Data availability This manuscript has associated data available online on data repository. [Authors' comment: The ALICE experimental data are taken from <https://www.hepdata.net/> from the papers <https://doi.org/10.17182/hepdata.61857> and <https://doi.org/10.17182/hepdata.62098>].

References

1. J. Adams et al., (STAR Collaboration) Nucl. Phys. A **757**, 102 (2005)
2. K. Adcox et al., (PHENIX Collaboration) Nucl. Phys. A **757**, 184 (2005)
3. M. Gyulassy et al., Nucl. Phys. A **750**, 30 (2005)
4. J. Adam et al., Phys. Rev. C **95**, 064606 (2017)
5. P. Koch et al., Phys. Rept. **142**, 167 (1986)
6. J. Rafelski, Eur. Phys. ST **155**, 139 (2008)
7. K.A. Bugaev et al., Ukr. J. Phys. **61**, 8 (2016)
8. G. Bocquet et al., (UA1 Collaboration) Phys. Lett. B **366**, 441 (1996)
9. R.E. Ansorge et al., (UA5 Collaboration) Nucl. Phys. B **328**, 36 (1989)
10. R.E. Ansorge et al., (UA5 Collaboration) Phys. Lett. B **199**, 311 (1987)
11. R. Hagedorn, Riv. Nuovo Cim. **6**, 1 (1983)
12. J.D. Bjorken, FERMILAB–Pub–82/59–THY, USA (1982)
13. D. d’Enterria, R. Stock, **23**, 99 (2010)
14. S. Chatrchyan et al., (CMS Collaboration) Eur. Phys. J. C **72**, 1945 (2012)
15. B. Abelev et al., (ALICE Collaboration) Phys. Lett. B **720**, 52 (2013)
16. G. Aad et al., (ATLAS Collaboration) JHEP **09**, 050 (2015)

17. K. Aamodt, *et al.*, (ALICE Collaboration), *Phys. Lett.* **B696** (2011).
18. Z. Yin et al., (ALICE Collaboration) *Intl. J. Mod. Phys. Conf. Series* **29**, 1460228 (2014)
19. V. Khachatryan et al., (CMS Collaboration) *JHEP* **04**, 039 (2017)
20. J. Rafelski, *Eur. Phys. J. Spec. Top.* **155**, 139 (2008)
21. R.J. Fries et al., *Phys. Rev. C* **68**, 044902 (2003)
22. V. Topor et al., *Phys. Rev. C* **70**, 064906 (2004)
23. S.J. Brodsky et al., *Phys. Lett. B* **668**, 111 (2008)
24. C. Shen et al., *Comput. Phys. Commun.* **199**, 61 (2016)
25. W. Zhao et al., *Eur. Phys. J. C* **77**, 645 (2017)
26. S. McDonald et al., *Phys. Rev. C* **95**, 064913 (2017)
27. V. Greco et al., *Phys. Rev. Lett.* **90**, 202302 (2003)
28. R.J. Fries et al., *Phys. Rev. Lett.* **90**, 202303 (2003)
29. V. Minissale et al., *Phys. Rev. C* **92**, 054904 (2015)
30. A. Arif, Y. Ali, M.Q. Haseeb, *Eur. Phys. J. Plus* **136**, 737 (2021)
31. A. Arif et al., *Int. J. Mod. Phys. E* **30**, 2150068 (2021)
32. A. Arif, Y. Ali, *Eur. Phys. J. Plus* **136**, 951 (2021)
33. M. Šefcík, et al., (ALICE Collaboration) *EPJ Web Conf.* **171** 13007 (2018)
34. P. Kalinak, (ALICE collaboration) *EPS-HEP* (2017)
35. T. Pierog, K. Werner, *The EPOS Model, Proceedings of the 31st ICRC, Lodz* (2009)
36. T. Pierog et al., *Phys. Rev. C* **92**, 034906 (2015)
37. K. Werner et al., *Phys. Rev. C* **74**, 044902 (2006)
38. M. Hladik et al., *Phys. Rev. Lett.* **86**, 3506 (2001)
39. N.N. Kalmykov et al., *Russ. Acad. Sci. Phys.* **58**, 1966 (1994)
40. R.J. Fries, *J. Phys. G* **30**, S853 (2004)
41. K. Werner, *Nucl. Phys. B* **81**, 175 (2008)